Check for updates

Original Research Article

JOURNAL OF COMPOSITE MATERIALS

Journal of Composite Materials
2025, Vol. 0(0) 1–20
© The Author(s) 2025

Article reuse guidelines:
sagepub.com/journals-permissions
DOI: 10.1177/00219983251405993
journals.sagepub.com/home/jcm
Sage

Permeability characterization of a biaxial stitched fabric: Insights from 2D flow experiments under unsteady and steady flow regimes

Hasan Caglar[1] and **Ercument Murat Sozer**[2]

Abstract

This study investigated in-plane permeability of a biaxial stitched E-glass fabric preform using 2D (radial) flow experiments under constant-injection pressure at fiber volume fractions of $V_f = 41–54\%$. Unsteady permeability was determined through a repeated set of experiments on separate specimens and by tracking elliptical flow front propagation with time along x, y axes and $\theta = 45°$. The fabric exhibited an anisotropic behavior with unsteady permeability along the production line (x-direction) being significantly higher than permeability along the transverse line (y-direction). The ratios of principal permeability components, $\frac{K_{uns,1}}{K_{uns,2}}$ were 5.67 ± 2.14, 3.72 ± 0.90 and 3.97 ± 0.87 at $V_f = 0.41$, 0.46 and 0.54, respectively. For steady permeability characterization, analytical relationship (driven from Darcy's Law) between the permeability and process parameters (inlet hole diameter, resin viscosity, inlet and exit pressures) is usable only if the exit flow rate is measured at an elliptical mold edge, which is not practical as these characterization experiments are usually conducted with a non-elliptical mold (circular or square). In this study, steady permeability was calculated by using experimental steady flow rate, an assumption that the anisotropy ratio calculated in the unsteady regime remains constant at steady state, and a straightforward numerical iterative solution. The ratio of steady to unsteady permeabilities, $\frac{K_s}{K_{uns}}$ was determined as 0.97 ± 0.33, 0.76 ± 0.09 and 0.54 ± 0.26 at $V_f = 0.41$, 0.46 and 0.54, respectively. This study presents a valuable methodology and key insights into the permeability of a biaxial fabric, extendable to other fabric types and contribute to advancing the understanding and modeling of mold filling in liquid composite molding processes.

Keywords

2D permeability, biaxial fabric, numerical solution, composite manufacturing

Introduction

Resin Transfer Molding (RTM) process is traditionally utilized for producing thermoset matrix composites. Recently, a newer generation process, thermoplastic resin transfer molding (TP-RTM) has been employed in the manufacturing of thermoplastic matrix (e.g., Elium®, anionically polymerised Polyamide 6) composites due to their distinct properties such as superior toughness and weldability, making them suitable for applications where thermoset matrix may not meet the expectations of impact resistance and part assembly.[1–3] Regardless of whether the matrix is thermoset or thermoplastic, successful RTM processing relies on a thorough understanding of resin flow through a porous fiber reinforcement. Consequently, characterizing the permeability of porous fiber reinforcements is essential for accurately modeling mold filling in Liquid Composite Molding (LCM) processes. In these processes, a liquid polymer (resin) impregnates a dry fiber reinforcement (typically made of stacked fabric layers) placed in a mold cavity prior to resin injection (as in Resin Transfer Molding, RTM) or resin infusion (as in Vacuum-Assisted RTM, VARTM, also known as Resin Infusion, RI). Simulation of mold filling is done through mathematical modeling of porous media flow based on Darcy's Law and its numerical solution. This is highly beneficial, as it helps predict resin flow and optimize key manufacturing parameters. These include the placement of gates (resin inlets and outlets),

[1]School of Aerospace, Transport and Manufacturing, Centre for Materials, Cranfield University, Bedford, UK
[2]Mechanical Engineering Department, Koc University, Istanbul, Turkey

Corresponding author:
Ercument Murat Sozer, Mechanical Engineering Department, Koc University, Rumelifeneri Yolu, Sariyer 34450, Istanbul, Turkey.
Email: msozer@ku.edu.tr

Data Availability Statement included at the end of the article.

boundary conditions (such as pressure levels or flow rates), and the timing for opening or closing valves. Simulation is especially useful when: (1) the composite part has a large or complex geometry, or (2) there are significant variations in the fiber volume fraction and permeability of the fabric preform.[4] The reliability of simulation results strongly depends on the accuracy of the permeability data. Regional variations (such as much higher permeability of mold cavity along edge race-tracking channels than inner regions) may drastically affect resin flow pattern. Random and minor variations (such as a few missing yarns or unintended shearing during fabric placement) can locally affect permeability due to changes in dual-scale porosity, but they typically do not have a significant impact on the overall mold filling pattern.[5,6] Mold filling simulations are primarily used to ensure complete mold filling (by minimizing air entrapment and thus no significant void remains in the preform) and shorten manufacturing cycle time by designing fast mold filling and resin cure. Simulations replace time-consuming and costly experimental trial-and-error approaches during designing mold and process parameters.[7] To model mold filling of thick composite parts, through-thickness permeability (besides in-plane permeability components) must also be characterized for 3D flow simulations.[8,9] However, as the thickness of the mold cavity is usually much smaller than the in-plane dimensions, 2D mold filling models for resin injection or infusion processes are commonly preferred over 3D models due to their simplicity. Accurate permeability measurement is essential for reliable flow simulations, and therefore plays a critical role in mold design (e.g., gate and vent placement) as well as in setting the processing window (boundary conditions such as injection and venting pressures)[4] and advancing composite material manufacturing applications such as wind turbine blades,[10] tidal turbine blades[11–13] and aircraft wings and wingbox.[14] All of these factors make accurate permeability measurement a subject of significant importance and ongoing research in composite manufacturing.

For porous-media flows, conservation of momentum equation of fluid mechanics is replaced with the following empirical Darcy's Law in 2D modeling:

$$\overline{U} = \begin{Bmatrix} \overline{u} \\ \overline{v} \end{Bmatrix} = -\frac{[K]}{\mu} \circ \nabla P = -\frac{1}{\mu} \begin{bmatrix} K_{xx} & K_{xy} \\ K_{yx} & K_{yy} \end{bmatrix} \begin{Bmatrix} \frac{\partial P}{\partial x} \\ \frac{\partial P}{\partial y} \end{Bmatrix} \quad (1)$$

where $\overline{U}$ is the resin velocity (a.k.a. the volume averaged Darcy's velocity), ∇P is the resin pressure gradient, μ is the resin viscosity and $[K]$ is the permeability tensor of the porous medium (reinforcement fabric) with a usually common assumption of orthotropic material, $K_{xy} = K_{yx}$.[4] This law allows modelers to use a macroscopic relationship between velocity and pressure gradient, instead of solving the conventional conservation of momentum equations in micro channel network in a macroscale porous medium. A modeler needs in-plane permeability components: either K_{xx}, K_{yy} and K_{xy} (usually aligned with respect to fabric roll's production and transverse directions) or $K_{uns,1}$ and $K_{uns,2}$ along principal (major and minor) axes. Two general approaches are available in literature: (1) experimental measurement and (2) prediction based on modeling and numerical solution. Various dimensional configurations, flow regimes and boundary conditions are used in experiments: in-plane (1D or 2D) or out-of-plane (a.k.a. through-thickness); unsteady or steady flow; and constant-pressure or constant-flow rate at the inlet. Best curve-fit (driven from Dracy's Law) is applied to the data collected.[15] Each approach has advantages and disadvantages over others. Hence, there is no clear consensus in literature on permeability characterization (unsteady or steady; under constant injection pressure or flow rate; 2D (radial) or a set of 1D). Measuring both unsteady and steady permeabilities sequentially on the same specimen presents challenges mainly due to the difficulty of simultaneously assessing permeability in multiple directions using a single setup, unless separate one-dimensional measurements are performed in each direction. Two-dimensional (a.k.a. radial) flow experiments (typically conducted in a flat mold with a circular central inlet gate) are widely used to measure in-plane permeability. Flow front's radial position is tracked along three directions (x, y and $\theta = 45°$). The principal permeability components are derived from the elliptical flow front shape. It is advantageous that 2D (radial) experiments allow determining principal axes and permeability components in those directions, simultaneously in a single experiment. However, a general trend is to repeat experiments on separate specimens to investigate statistical variations in permeability caused by fabric irregularity and inconsistent labor (cutting and stacking of fabric layers).

Swery et al.[16] measured both 2D unsteady and steady permeabilities for plain woven E-glass fabric by assuming that the fabric is isotropic during steady flow regime. Buntain et al.[17] measured the steady permeability of an isotropic fabric preform at various fiber volume fractions (V_f) using radial flow experiments. For each experiment of this continuous process, they fixed V_f, measured the permeability, then adjusted V_f to a new value and repeated the process. Similarly, Comas-Cardona et al.[18] measured continuous permeability of an E-glass twill-weave and carbon non-crimp fabrics by using the anisotropy ratio obtained from a prior measurement. Many studies on 2D permeability predominantly focus on unsteady permeabilities, omitting the measurement of steady permeability in the same experimental context.

Using unsteady permeability may seem to be more appropriate than steady permeability, especially while simulating flow front propagation in LCM (which is an unsteady

process itself). Different than steady (and thus saturated) flow regime, many experimental unsteady studies revealed that full saturation behind flow front takes extra time due to delayed saturation of microvoids especially in intra tow spaces which are typically less porous and permeable than inter tow spaces. However, Darcy's Law assumes full saturation of the preform behind the resin flow front. Steady permeability measurements should be preferred while simulating the resin pressure and velocity distributions during post-filling stages such as resin bleeding.[17] As demonstrated in a radial permeability benchmark study,[19] the variations between repeated experiments—whether conducted by the same experimenter or different participants—can be substantial, often reaching ±20% and sometimes differing by an order of magnitude. The common reasons for these variations are fiber tow nesting and shearing, tool deflection, preforming defects and inherent textile defects.[6] Therefore, mold filling simulations are essential for understanding the injection and infusion processes; however, their accuracy is highly sensitive to uncertainties in the permeability of the reinforcements.

In this study, both 2D unsteady and steady permeabilities of a biaxial fabric were characterized and compared at three different fiber volume fractions (V_f = 41–54%) under constant-injection pressure boundary condition at the central inlet hole. Unsteady characterization was done by tracking and analyzing evolution of elliptical flow front. For various fabric types, this approach was previously well documented in many studies in literature[7,16,18–20] using a closed-form relationship (driven from Darcy's Law) between dependent variables (radii of the major and minor axes of the elliptical flow front, or more commonly along x, y and θ = 45° directions), independent variable (time) and parameters of experiment (porosity of a fabric specimen, resin viscosity, inlet hole radius and constant-injection pressure). However, to the best of our knowledge, no anisotropic 2D steady-state permeability characterization has been reported in the literature because typical fabric specimens used in characterization experiments are usually circular or square, and thus implementing exit boundary condition of a steady flow analysis becomes analytically ambiguous or inapplicable. That means, the boundary condition (resin exit pressure, $P_{exit} = P_{atm}$ absolute pressure = 0 gage pressure) is not at an elliptical flow front, but at a circular or square edges of a specimen.

Recall that 2D (radial) unsteady permeability characterization is preferred over 1D alternative because 1D characterization is more time-consuming (a pair of experiments is needed instead of a single one). In other words, 2D characterization is quicker as it allows measuring K_{xx}, K_{yy} and $K_{45°}$ (and thus K_1 and K_2) simultaneously. However, this is true only for unsteady characterization, but not for the steady case due to the ambiguity of the exit boundary condition.

The proposed approach in this study (a combination of experimental data (flow rate) and an iterative numerical analysis) overcomes the abovementioned issue by computing the exit velocity components along all edges and flow rate for fabric specimens in non-elliptical molds.

In this study, unsteady (also referred to as transient or unsaturated) permeability was measured experimentally, while steady (also referred to as saturated) permeability was predicted through simulation. The former was determined by curve fitting the experimental data of the radial flow front position, $r(t)$, versus time along three directions (x, y, and θ = 45°), using the closed-form relationship between the permeability components and the evolution of the flow front position.[19,21] By using Finite Difference Method (FDM), the latter was determined under steady-state conditions by iteratively solving the pressure distribution in the fully filled mold cavity and matching the numerical flow rate with the experimental one.

The present study will be helpful to measure 2D steady permeability components with the following steps: (1) it is assumed that the anisotropy ratio of unsteady permeability components and the rotation angle between x-y and principal 1–2 axes remains unchanged at steady state, and (2) permeability values are numerically iterated by calculating exit velocity components along all edges and matching the corresponding flow rate ($Q_{numerical}$) to the experimentally measured flow rate in the characterization experiment ($Q_{experiment}$).

Subsequent sections provide comprehensive information on the materials, the 2D permeability measurement setup, and present both experimental and numerical results, discussion and conclusions.

Materials and procedure of permeability characterization experiments

Materials

Permeability characterization of a biaxial stitched E-glass fabric (Metyx LT850 0/90, see Figure 1) was conducted at different fiber volume fractions by stacking five layers in a varying mold thickness, h. A new fabric specimen was used in each experiment. Silicone oil (Xiameter PMX 200) was used as test fluid. Material properties (oil viscosity and fabric superficial density per layer) are given in Table 1. During each experiment, the temperature of the silicone oil was recorded by using a thermocouple sensor. Temperature-dependent viscosity characterization for the oil was previously conducted by Technical University of Munich as a part of a benchmark study.[19] The Arrhenius equation, $\mu = Ae^{\frac{-E_a}{RT}}$ was fitted to the experimental data using the least square method, where R is the universal gas constant (= 8.3144598 J/°K.mol) and the determined constants are A = 2.8858×10^{-4} Pa.s and $E_\alpha = -1.4376 \times 10^4$ J/mol.

Experimental procedure

Five layers of the fabric with in-plane dimensions of 0.21 m × 0.21 m were cut and stacked with a sequence of $[0]_5$. To create an inlet for the resin injection, the center of the fabric preform was punched with a hole diameter of 12 mm. Sharp hole edge was assumed to allow major flow in in-plane directions, and prevent significant resin flow through the thickness direction of the fabric during its initial entry into the mold cavity and throughout the impregnation of a specimen. A preformed specimen was placed on a lower metallic mold half (see Figure 2(b)). Eight steel spacers were placed between the lower and upper mold halves to adjust the cavity thickness. Three cavity thicknesses were studied: h = 3.0, 3.5, and 4.0 mm. An upper mold half made of perforated aluminum plate with glass monitoring windows was compressed onto the preform using 16 latches and 8 clamps (see Figures 2 and 3).

Compressed air pressurized the resin in a pressure pot to the targeted injection value of 80 kPa. An analog pressure regulator (CKD RP1000) was used to set this value. The resin pressure and temperature were recorded using a pressure sensor (Keller PAA 35X, 0 to 10 bar abs, 0.002 full scale resolution) and a thermocouple, respectively. Although the experiments were conducted under isothermal room temperature condition, the viscosity of the resin was calculated by averaging the temperature of the resin (T) recorded during each experiment (not a significant temperature variation was observed during any experiment) and substituting it in the Arrhenius equation, $\mu = Ae^{\frac{-E_a}{RT}}$ with the constants tabulated in Table 1.

Resin injection was facilitated from the center of the lower mold half, and the outlet vent was open to the atmosphere (see Figure 2). In this study, an anisotropic biaxial fabric preform was used, consequently an elliptical flow front was observed (Figure 4). The flow front radii in three directions (r_{xx}, $r_{45°}$ and r_{yy}) were recorded through the glass inspection region (Figure 3(a)) using a digital camera until the resin started flushing out from the outlets. Afterwards, resin bleeding stage took place until the flow rate became steady. The first data point for unsaturated permeability measurement was recorded approximately 2 s after resin first became visible at the inlet hole. During the initial 2-s period, the resin flow front advanced rapidly (on the order of several centimeters), and this short delay in data collection was assumed to ensure that entry effects associated with the punched hole had diminished.

The components of 2D unsteady permeability (K_{uns}) along three directions (depicted as $K_{uns,xx}, K_{uns,45°}$ and $K_{uns,yy}$ (a.k.a. $K_{uns,0°}, K_{uns,45°}$ and $K_{uns,90°}$) along x, θ = 45° and y directions, respectively) of a fabric preform under constant-injection pressure were determined using the following equations[21]:

$$K_{uns,xx} = C\left\{r_{f,xx}^2\left(2\ln\left(\frac{r_{f,xx}}{r_i}\right) - 1\right) + r_i^2\right\}\frac{1}{t} \quad (2a)$$

$$K_{uns,45°} = C\left\{r_{f,45°}^2\left(2\ln\left(\frac{r_{f,45°}}{r_i}\right) - 1\right) + r_i^2\right\}\frac{1}{t} \quad (2b)$$

$$K_{uns,yy} = C\left\{r_{f,yy}^2\left(2\ln\left(\frac{r_{f,yy}}{r_i}\right) - 1\right) + r_i^2\right\}\frac{1}{t} \quad (2c)$$

where the coefficient C is defined as $C = \frac{\mu\phi}{4P_{inj}}$ where μ is the viscosity of the silicone oil, ϕ is the porosity (= $1 - V_f$) of the fabric preform, r_f is the flow front radii (stated as $r_{f,xx}$, $r_{f,45°}$ and $r_{f,yy}$ along x, θ = 45° and y directions, respectively), r_i is the inlet hole radius (0.006 m), t is time, P_{inj}

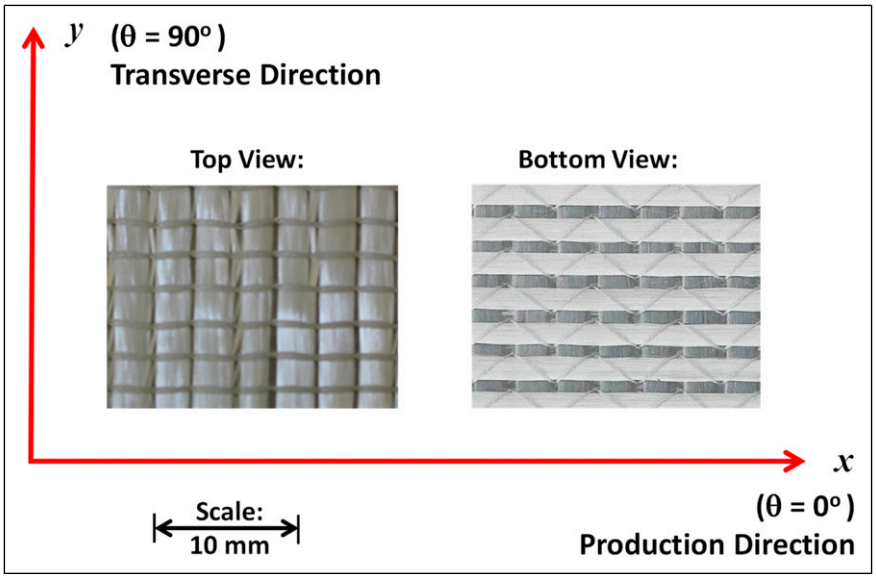


Figure 1. Top and bottom views of Metyx LT850 0/90 E-glass biaxial stitched fabric.

Table 1. Material properties of the resin and fabric[19].

Material	Properties	Value
Silicone oil (test fluid used as resin)	Viscosity, μ [Pa.s]	$\mu = Ae^{\frac{-E_\alpha}{RT}}$ where R = 8.3144598 J/°K.mol $A = 2.8858 \times 10^{-4}$ Pa.s $E_\alpha = -1.4376 \times 10^4$ J/mol[11]
Biaxial fabric (0°/90°)	Superficial density per layer, ρ_{sup} [g/m^2]	850
	Number of layers, n	5
	Stacking sequence	$[0]_5$
	Bulk density of glass fibers, ρ_{bulk} [kg/m^3]	2540

(gage pressure relative to atmospheric pressure) is the injection pressure at the inlet. These unsteady permeability components were determined with the least square method by fitting a first order polynomial to the experimental data corresponding to the terms preceding $1/t$ on the right-hand-sides of equations ((2a)–(2c)) versus time.

The first data point for unsaturated permeability measurement was recorded approximately 2 s after resin first

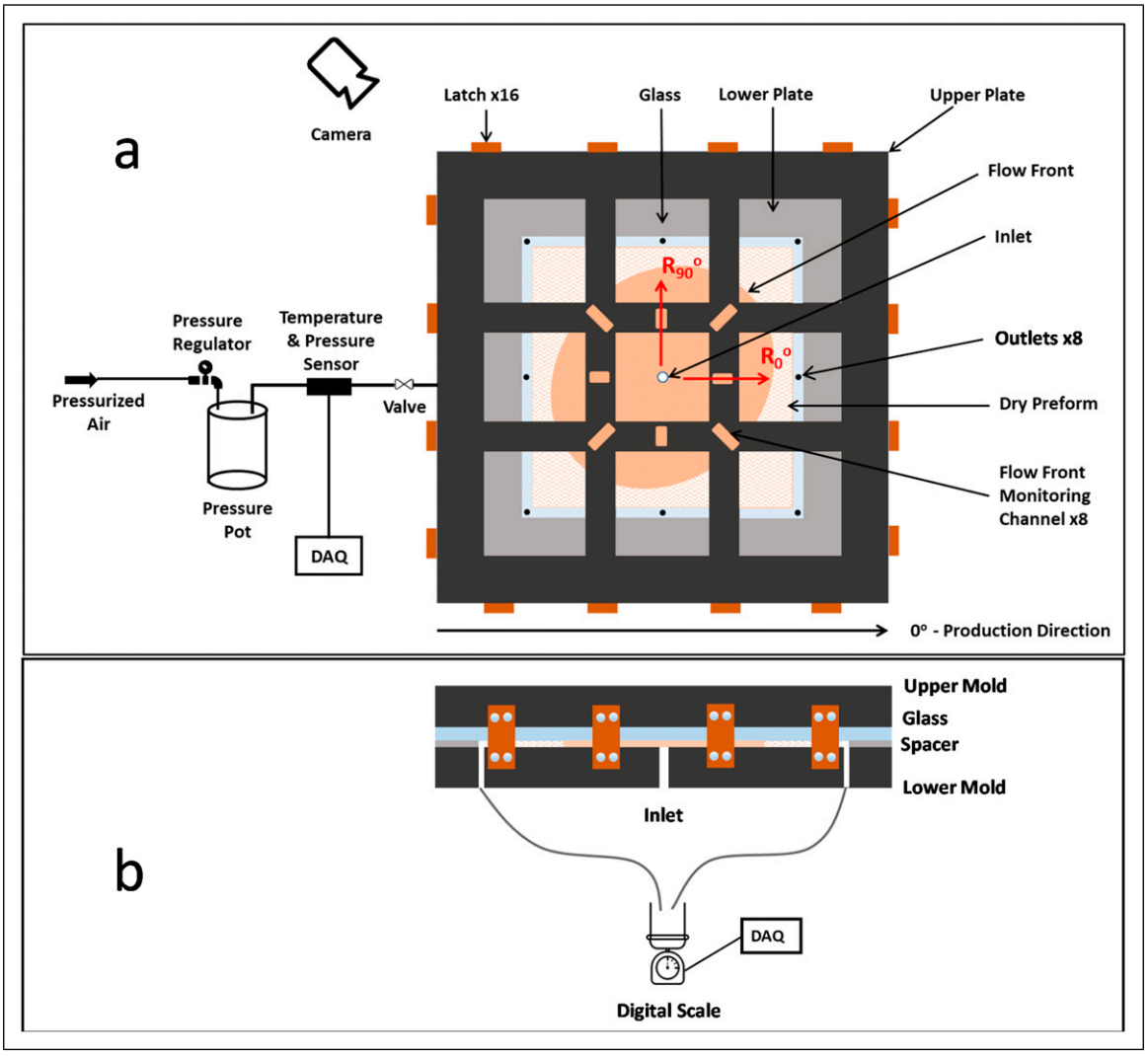


Figure 2. 2D (radial) permeability measurement setup: (a) top view and (b) side view. Transient (unsteady) flow regime is illustrated here where the elliptical flow front has not reached the exit pool along the mold edges yet.

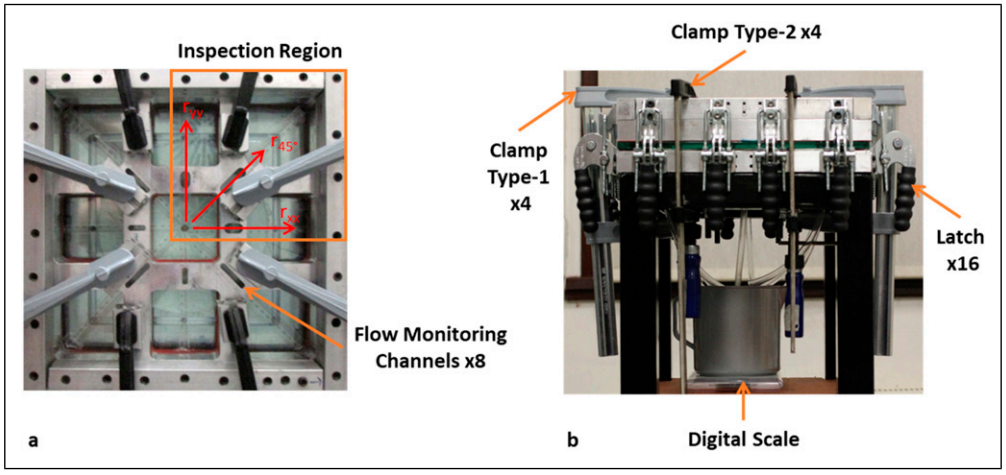


Figure 3. 2D (radial) permeability measurement setup: (a) top view and (b) side view.

became visible at the inlet hole. During this period, the resin flow front advanced rapidly (on the order of several centimeters), and this short delay in data collection was assumed to ensure that entry effects associated with the punched hole had diminished. The experimental data was obtained by post-processing of the video recordings manually. While curve-fitting, equations ((2a)–(2c)) were expressed as $K_{uns} = \frac{f(t)}{t} = \frac{Dt+E}{t}$ and observed that $K_{uns} \cong D$ for large t values (i.e., when the flow front propagated and thus became $r_f \gg r_i$). The associated coefficient of determination (R^2) was sufficiently high ($R^2 > 0.99$), indicating that the data were consistent with equation (2), which was previously derived under the assumptions of uniform permeability, radial flow through a porous medium governed by Darcy's law, and that the first data point was recorded when the flow front was reasonably far from the inlet.

As previously done in a benchmarking study,[21] axes transformation is done to determine the principal permeabilities (denoted as $K_{uns,1}$ and $K_{uns,2}$ here) and the rotation angle β between the axes x–y and 1–2 using the following equations (see Figure 4):

$$K_{uns,1} = K_{uns,xx} \frac{\alpha_1 - \alpha_2}{\alpha_1 - \frac{\alpha_2}{\cos(2\beta)}} \tag{3}$$

$$K_{uns,2} = K_{uns,yy} \frac{\alpha_1 + \alpha_2}{\alpha_1 + \frac{\alpha_2}{\cos(2\beta)}} \tag{4}$$

$$\beta = \frac{1}{2}\tan^{-1}\left(\frac{\alpha_1}{\alpha_2} - \frac{{\alpha_1}^2 - {\alpha_2}^2}{\alpha_2 K_{uns,45^\circ}}\right) \tag{5}$$

where

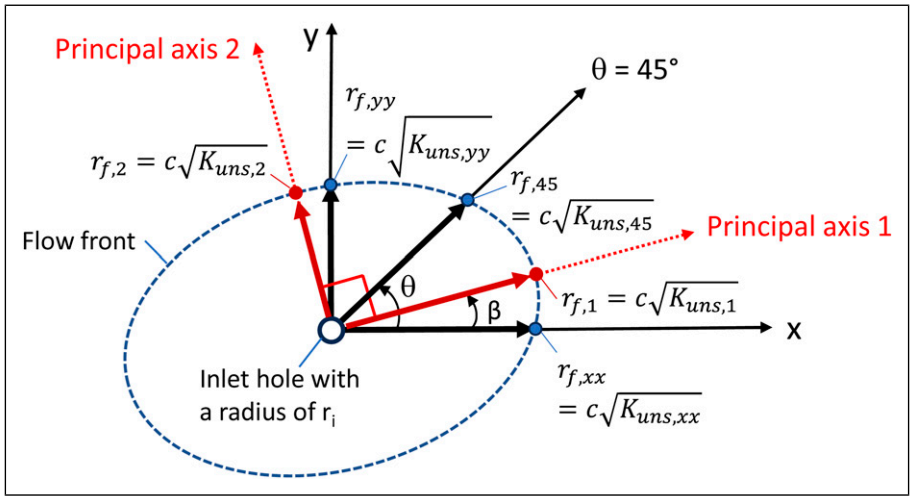


Figure 4. Coordinate systems x–y and 1–2. The three radii $r_{f,xx}$, $r_{f,45^\circ}$ and $r_{f,yy}$ of the elliptical flow front are tracked and used to calculate the unsteady permeability components $K_{uns,xx}$, $K_{uns,45^\circ}$ and $K_{uns,yy}$, along x, θ = 45° and y directions, respectively.

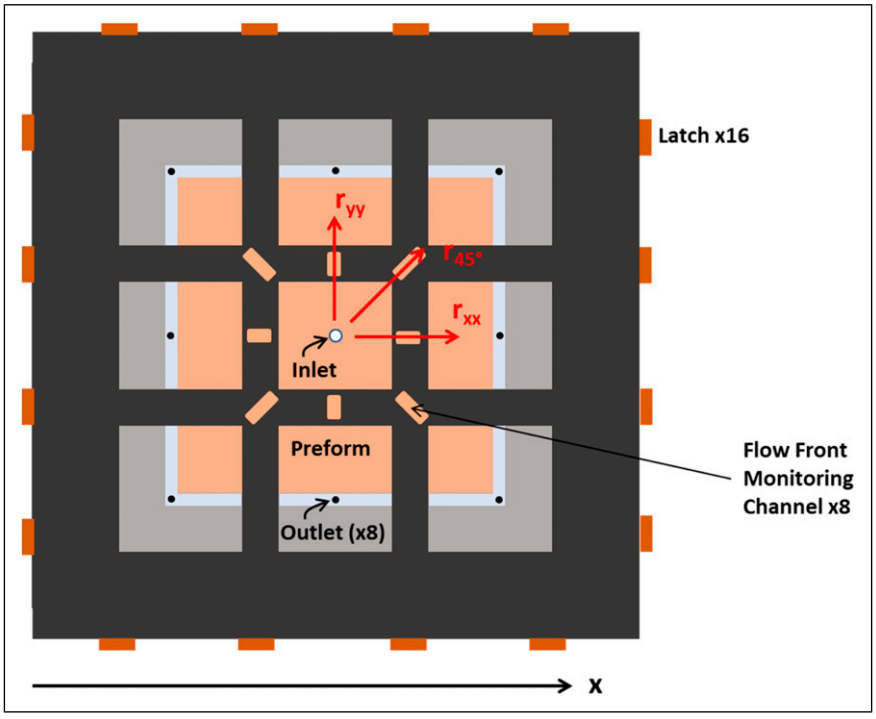


Figure 5. Top view of the 2D (radial) permeability measurement setup schematically showcasing a steady flow regime, i.e., when the fabric preform was fully wetted.

$$\alpha_1 = \frac{K_{uns,xx} + K_{uns,yy}}{2} \quad \text{and} \tag{6a}$$

$$\alpha_2 = \frac{K_{uns,xx} - K_{uns,yy}}{2} \tag{6b}$$

As in this study, if one uses x–y coordinate system (instead of 1–2 coordinate system) in the numerical solutions, $K_{uns,xy}$ ($= K_{uns,yx}$ due to a symmetric tensor assumption) term is needed, which can be calculated as follows[22]:

$$K_{uns,xy} = \frac{K_{uns,1} - K_{uns,2}}{2}\sin(2\beta) \tag{7}$$

The anisotropy ratio, $K_{uns,1}/K_{uns,2}$ is obtained by dividing equation (3) by equation (4) and simplifying the result as follows:

$$\frac{K_{uns,1}}{K_{uns,2}} = \frac{K_{uns,xx}}{K_{uns,yy}}\frac{\alpha_1 - \alpha_2}{\alpha_1 + \alpha_2}\frac{\alpha_1 + \frac{\alpha_2}{\cos(2\beta)}}{\alpha_1 - \frac{\alpha_2}{\cos(2\beta)}} = \frac{\alpha_1 + \frac{\alpha_2}{\cos(2\beta)}}{\alpha_1 - \frac{\alpha_2}{\cos(2\beta)}} \tag{8}$$

Although the analysis was based only on data from the inspection region ($0° \le \theta \le 90°$), as is commonly done in the literature, the flow front in the other regions was also observed to follow a similar qualitative pattern, with its elliptical shape matching that of the analyzed quarter. The experimental setup included a peripheral groove surrounding the specimen, with eight outlets located within it on the lower mold plate (see Figure 5). The bled resin was collected in a container on a digital scale (see Figure 2 and 3), and the mass versus time data of the resin was recorded using a DAQ system on MATLAB®. After the resin bleeding was observed, the resin flow continued for at least 300 s to ensure complete impregnation of the fabric and thus to reach an almost steady flow. The data for the last 120 s were used in the calculation of the experimental volumetric flow rate, Q_{exp}. Mass flow rate, $\dot{m}$ was calculated as the slope of a first-order curve fit to the experimental data (the cumulative mass collected in the container vs time). Volumetric flow rate Q is $\dot{m}/\rho$ where ρ is the resin density.

Numerical modelling of 2D steady permeability

Following the numerical model and solution approach described in this section, the steady permeability components were determined in MATLAB® using a custom-written code, such that the simulated outflow volumetric flow rate matched the experimental measurements. The initial step in the analysis was the calculation of the pressure distribution. For 2D incompressible flow through a porous medium, the following continuity equation represents conservation of mass, assuming that both local inter- and intra-tow regions within a representative domain are filled simultaneously:

$$\frac{\partial \overline{u}}{\partial x} + \frac{\partial \overline{v}}{\partial y} = 0 \tag{9}$$

By assuming that the permeability tensor and viscosity are spatially uniform and $K_{s,xy} = K_{s,yx}$, substitution of equation (1) into equation (9) yields the following governing differential equation:

$$K_{s,xx}\frac{\partial^2 P}{\partial x^2} + K_{s,yy}\frac{\partial^2 P}{\partial y^2} + 2K_{s,xy}\frac{\partial^2 P}{\partial x \partial y} = 0 \tag{10}$$

$$K_{s,xx}\frac{P_W - 2P_C + P_E}{H^2} + K_{s,yy}\frac{P_S - 2P_C + P_N}{H^2} + 2K_{s,xy}\frac{P_{NE} - P_{SE} - P_{NW} + P_{SW}}{4H^2} = 0 \tag{11}$$

Here an inner central C node has indexes i and j for x and y axes, respectively such that $x = (i-1)\Delta x - L_x/2$ and $y = (j-1)\Delta y - L_y/2$. Leaving P_C alone results in the following expression for any inner point with $2 \le i \le N_x - 1$ and $2 \le j \le N_y - 1$

$$P_C = \frac{K_{s,xx}(P_W + P_E) + K_{s,yy}(P_S + P_N) + \frac{1}{2}K_{s,xy}(P_{NE} - P_{SE} - P_{NW} + P_{SW})}{2\left(K_{s,xx} + K_{s,yy}\right)} \tag{12}$$

Steady state pressure distribution, $P(x,y)$ was numerically calculated by discretizing the resin-filled domain (the entire mold; see Figure 7) and using finite-difference method (FDM). Pressure at any inner point was related to its neighbors' pressures when FDM was applied. By using $\Delta x = \Delta y \equiv H$, equation (10) was discretized as follows:

The pressure at the inlet hole was assigned as the injection pressure, and the pressure at the exit edges were assigned as atmospheric pressure (see Figure 6):

$$P = P_{inj} \text{ (at the inlet)} \tag{13}$$

$$P = P_{atm,gage} = 0 \text{ (at the exit)} \tag{14}$$

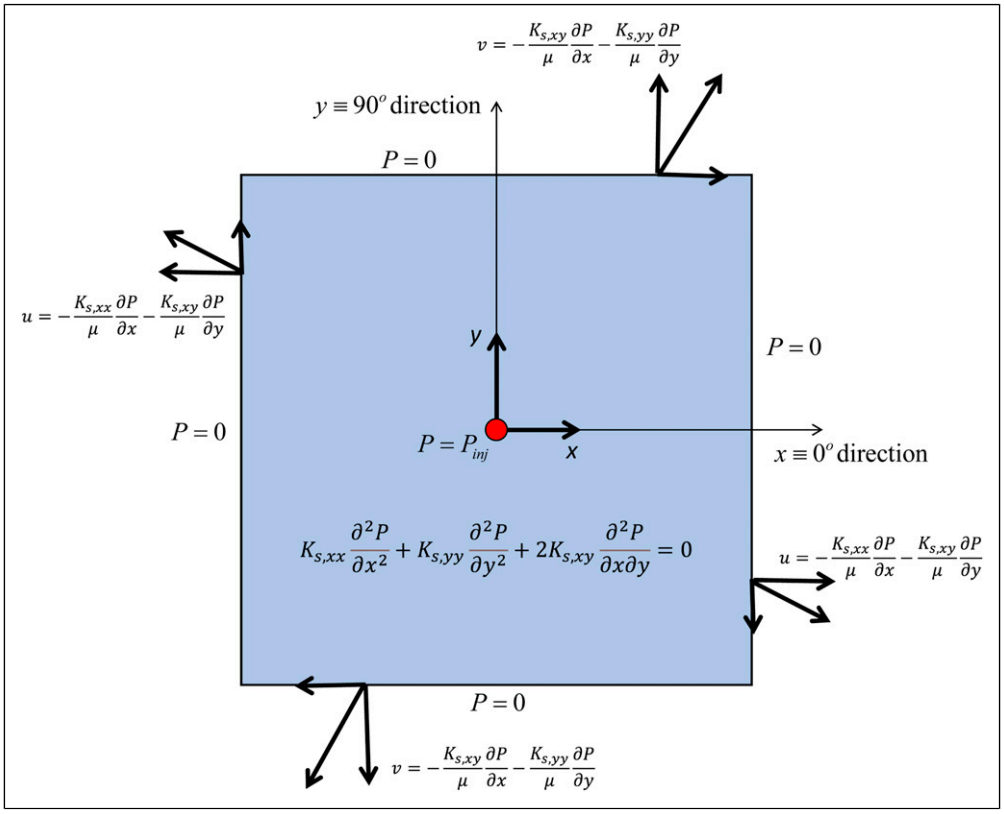


Figure 6. The domain of the fabric specimen wetted with resin at steady state 2D flow. Pressure boundary conditions were defined at the inlet hole and the outer periphery. Normal exit velocity components were specifically shown here and used to compute outflow rate at steady state.

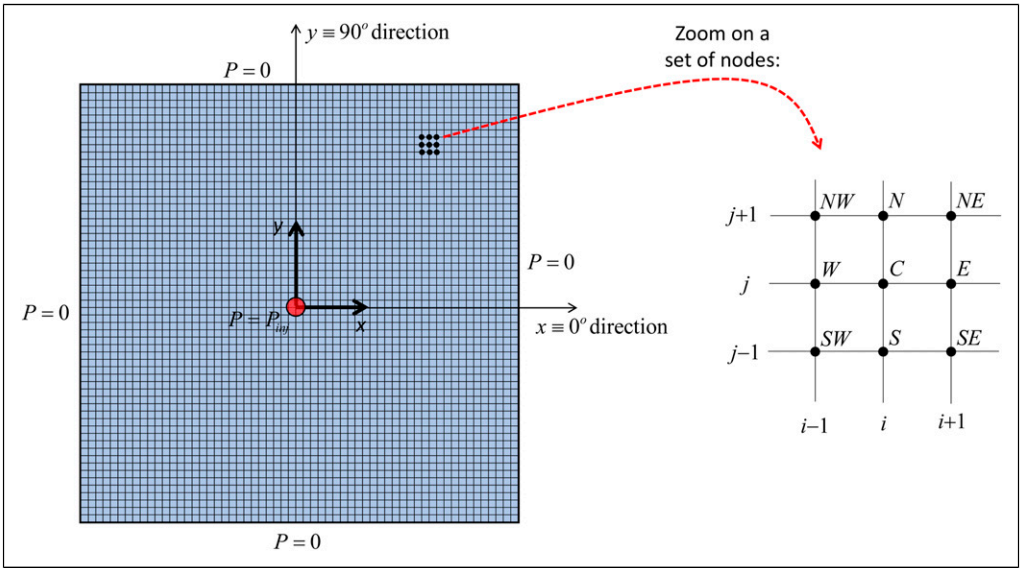


Figure 7. Grid and representative nodes used in finite difference method. Here a coarse mesh was illustrated, however, a finer grid with $N_x = N_y = 421$ (i.e., $\Delta x = \Delta y \equiv H = \frac{0.210\,\text{m}}{421-1} = 0.0005$ m) was used in all simulations. The representative nodes were named as C (Central), W (West), E (East), N (North), South (S), NW (North West), and so on.

These boundary conditions were numerically implemented as follows in the discrete form:

$$P = P_{inj} \text{ at all inlet nodes with } \sqrt{x_i^2 + y_j^2} \leq r_{in} \tag{15}$$

$$P = P_{atm,\,gage} = 0 \text{ at all exit boundary nodes with } i = 1, i = N_x, j = 1 \text{ and } j = N_y \tag{16}$$

The anisotropy ratio of the steady-state permeability tensor was assumed to remain unchanged from that of the unsteady-state permeability tensor:

$$\frac{K_{s,xx}}{K_{uns,xx}} = \frac{K_{s,yy}}{K_{uns,yy}} = \frac{K_{s,xy}}{K_{uns,xy}} = \frac{K_{s,1}}{K_{uns,1}} = \frac{K_{s,2}}{K_{uns,2}} = \text{constant} \equiv a \tag{17}$$

and thus the rotation angle between the two axes, β (see Figure 4) was assumed to remain unchanged too:

$$\beta_s = \beta_{uns} \tag{18}$$

During the initial unsteady stage of the characterization, the unsteady permeability was already experimentally measured. In the subsequent steady-stage analysis, the goal was to estimate the steady-state permeability components by iteratively determining the parameter a in equation (17). This iteration was based on matching the outflow rate computed numerically with that experimentally measured. The numerical volumetric outflow rate was calculated as follows:

$$Q_{num} = \int_A U \cdot \hat{n}\, dA \tag{19}$$

where A, U and $\hat{n}$ are the outer peripheral area of the fabric preform where the resin exits the mold, velocity and normal outward unit vector on A, respectively.

Iterative algorithm to estimate the steady permeability components. The algorithm used in the numerical procedure for estimating the steady permeability components was as follows:

(1) Initialization: Begin by predicting the steady permeability components $K_{s,xx}$, $K_{s,yy}$ and $K_{s,xy}$ by assigning $a = 1$ in equation (17).

Table 2. Convergence analysis conducted for Experiment 1.

Grid: $N_x \times N_y$	$\Delta x = \Delta y = H$ (m)	$\frac{K_{s,xx}}{K_{uns,xx}} = \frac{K_{s,yy}}{K_{uns,yy}} = \frac{K_{s,xy}}{K_{uns,xy}} = \frac{K_{s,1}}{K_{uns,1}} = \frac{K_{s,2}}{K_{uns,2}} \equiv a$	CPU time on a typical PC (s)
106 × 106	0.00200	0.4480	7
211 × 211	0.00100	0.4405	111
421 × 421	0.00050	0.4333	2218
841 × 841	0.00025	0.4279	34921

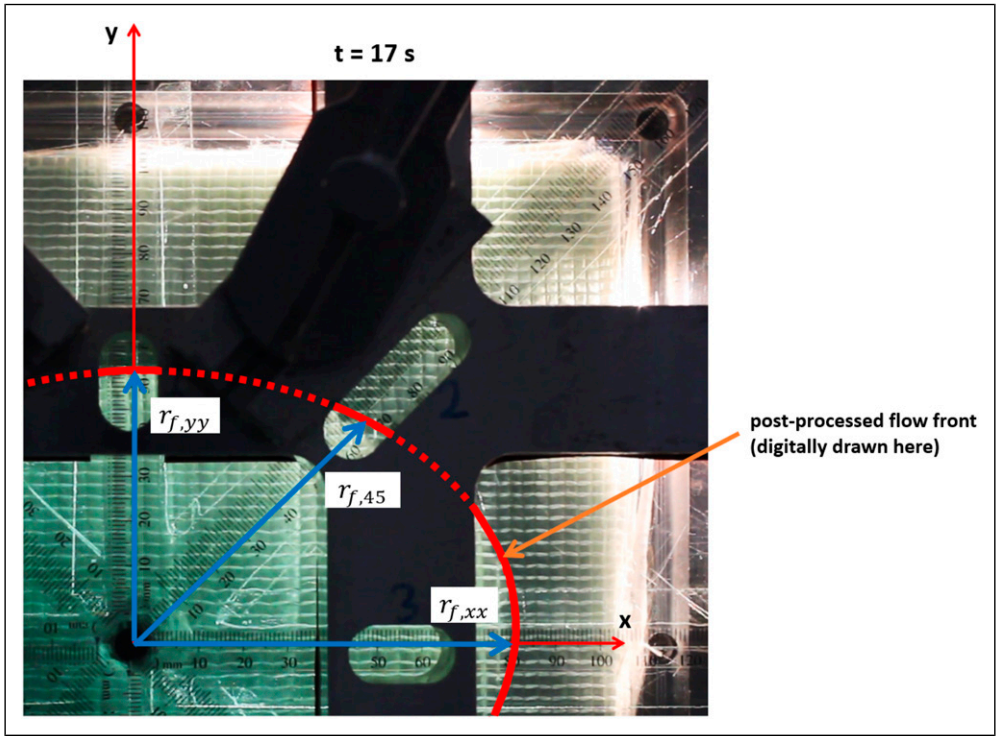


Figure 8. Elliptical flow front of resin at a sample instant.

(2) Pressure Field Solution: Solve the pressure distribution, $P(x,y)$ by numerically iterating pressure at each inner node (central, C) in terms of its surrounding nodal pressures in equation (12) and using the Finite Difference Method (FDM), subject to the boundary conditions defined in equations (15) and (16).
(3) Velocity Field Computation: Calculate the velocity components, $\overline{u}(x,y)$ and $\overline{v}(x,y)$ by using equation (1).
(4) Outflow Rate Computation: Calculate the numerical outflow rate, Q_{num} by using equation (19).
(5) Correction: Fix a in equation (17) by scaling it as follows: $a_{\text{new}} = a\frac{Q_{exp}}{Q_{num}}$.
(6) Permeability Update: Repeat the steps 1–3 by using the corrected a_{new}.

Although this procedure was referred to as an iterative solution method, it effectively involved only two steps (initial estimation and one correction) and can therefore be regarded as a quasi-direct approach.

Specifically, because both the velocity field (U) and the outflow rate (Q) are linearly proportional to the parameter a in equation (17), scaling the initially estimated permeability components by the ratio of $\frac{Q_{exp}}{Q_{num}}$ directly yielded the corrected steady permeability values.

Convergence analysis. A common finite difference method (FDM) grid was used across all 15 simulation experiments, based on a convergence study conducted for a representative case (Experiment 1). As the grid spacing H (see Figure 7) decreased, the ratio a appeared to converge (see Table 2). To balance accuracy with computational efficiency and thus avoid excessively long CPU times (e.g., 34,921/3600 = 9.7 h for an 841 × 841 grid in Experiment 1), a more practical grid size of 421 × 421 was chosen. This resolution was considered sufficient for achieving convergence to two significant figures in a (0.43 ∓ 0.01 for Experiment 1) which is the level of accuracy reported in Table 4 in the next section.

Results and discussion

Unsteady-state characterization

Recorded video of each experiment was post-processed to monitor the flow front propagation with time (see Figure 8 for an example). The results were discussed below.

- Permeability components in x–y coordinate system: For the fabric specimen used in this study, resin flow front was an elliptical shape at any instant of mold filling due to a strong anisotropy (as seen in Figure 9 for all of the 15 experiments). This confirms that resin flow was faster in x-direction than y-direction. As seen in Table 3, $K_{uns,xx}$ was measured as $5.06 \pm 0.60 \times 10^{-10}$, $2.32 \pm 0.43 \times 10^{-10}$ and $8.52 \pm 2.02 \times 10^{-11}$ m^2 (presented as the mean plus/minus one standard deviation of the five experiments) at $V_f = 0.408 \pm 0.002$, $V_f = 0.464 \pm 0.003$ and

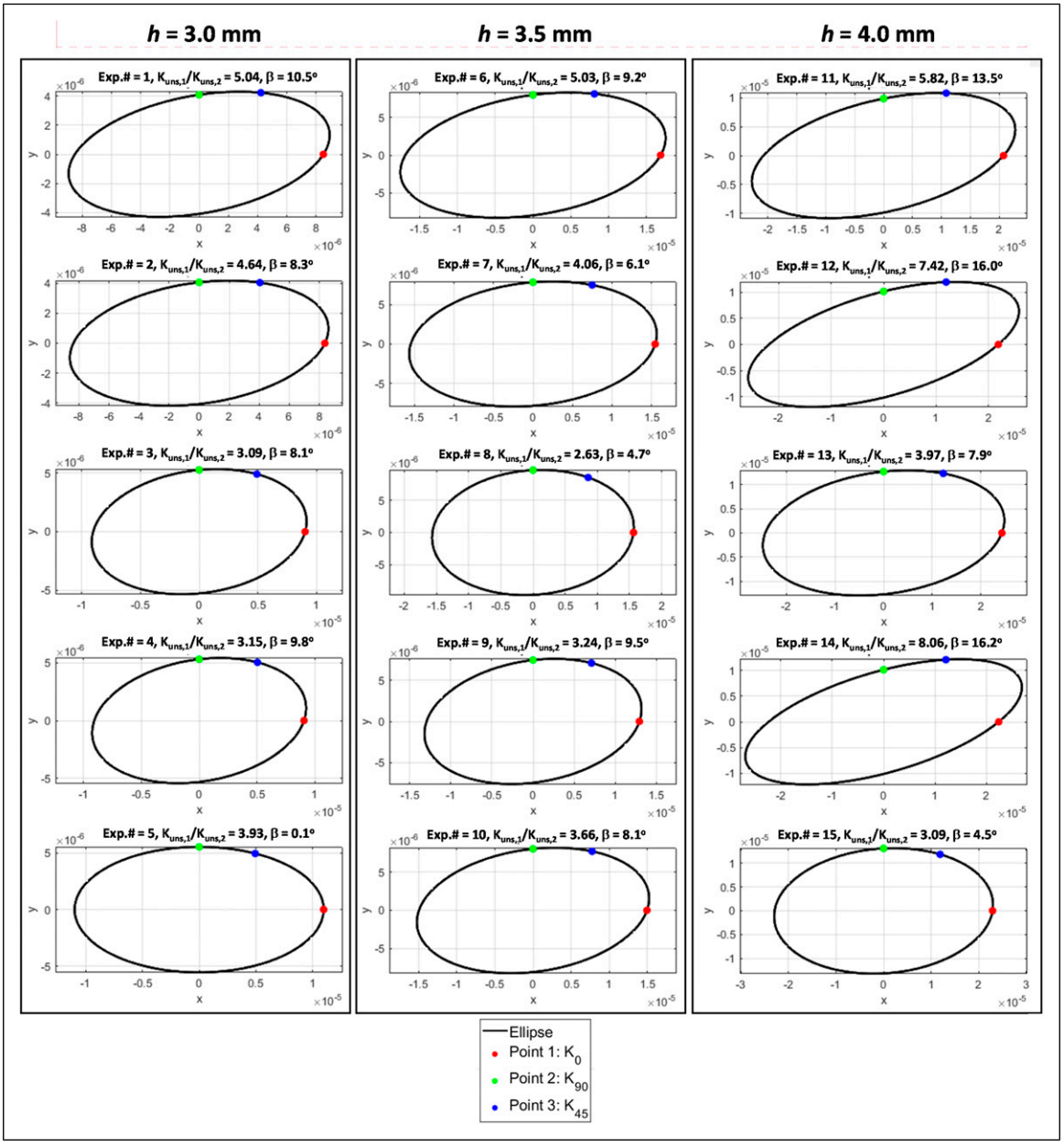


Figure 9. Analyses of the unsteady flow front propagation.

$V_f = 0.543 \pm 0.007$, respectively. The corresponding values of $K_{uns,yy}$ were $1.27 \pm 0.36 \times 10^{-10}$, $6.81 \pm 1.51 \times 10^{-11}$ and $2.40 \pm 0.68 \times 10^{-11}$ m^2. Off-diagonal term of the permeability tensor, $K_{uns,xy}$ was calculated using equation (8) and found to be not negligible, but significantly high (see Table 3).

- Principal permeability components in 1–2 coordinate system: As listed in Table 4, $K_{uns,1}$ was measured as $6.38 \pm 1.05 \times 10^{-10}$, $2.44 \pm 0.49 \times 10^{-10}$ and $8.98 \pm 1.75 \times 10^{-11}$ m^2 and $K_{uns,2}$ was measured as $1.23 \pm 0.39 \times 10^{-10}$, $6.73 \pm 1.54 \times 10^{-11}$ and $2.36 \pm 0.68 \times 10^{-11}$ m^2 at $V_f = 0.408 \pm 0.002$, $V_f = 0.464 \pm 0.003$ and $V_f = 0.543 \pm 0.007$, respectively. The rotation angle, β between x–y and 1–2 coordinate systems was calculated as $11.6° \pm 5.2°$, $7.5° \pm 2.1°$ and $7.4° \pm 4.2°$ at $V_f = 0.408 \pm 0.002$, $V_f = 0.464 \pm 0.003$ and $V_f = 0.543 \pm 0.007$, respectively.
- As illustrated in Figure 10, the **anisotropy** ratio, $K_{uns,1}/K_{uns,2}$ was determined as 5.67 ± 2.14, 3.72 ± 0.90 and 3.97 ± 0.87, at $V_f = 0.408 \pm 0.002$, $V_f = 0.464 \pm 0.003$ and $V_f = 0.543 \pm 0.007$, respectively. This strong **anisotropy** could stem from one major reason. The overall porosity in the x

Table 3. Parameters used in permeability experiments; and permeability components in *x–y* coordinate system. Std and CV stand for the standard deviation and coefficient of variation, respectively.

Exp.#	h (m)	Pinj (Pa)	Vf	T (C)	mu (Pa.s)	mdot (g/s)	Q (m^3/s)	Ku00	Ku45	Ku90	Kuxy
1	0.0030	79600	0.533	23.9	0.0974	0.0783	8.12e−08	7.22e−11	3.57e−11	1.67e−11	1.18e−11
2	0.0030	80400	0.552	21.9	0.1013	0.1009	1.05e−07	7.00e−11	3.27e−11	1.65e−11	8.39e−12
3	0.0030	79700	0.545	23.3	0.0985	0.1712	1.78e−07	8.14e−11	4.83e−11	2.78e−11	7.96e−12
4	0.0030	79400	0.540	23.4	0.0982	0.1978	2.05e−07	8.22e−11	5.09e−11	2.83e−11	9.94e−12
5	0.0030	78900	0.547	24.8	0.0957	0.0495	5.13e−08	1.20e−10	4.87e−11	3.05e−11	9.60e−14
Mean		79600	0.543	23.5	0.0982	0.1195	1.24e−07	8.52e−11	4.33e−11	2.40e−11	7.64e−12
Std		543	0.007	1.1	0.0020	0.0627	6.51e−08	2.02e−11	8.40e−12	6.80e−12	4.48e−12
CV		0.7	1.3	4.5	2.1	52.5	52.5	23.7	19.4	28.4	58.6
6	0.0035	79100	0.464	22.9	0.0993	0.5814	6.03e−07	2.85e−10	1.32e−10	6.38e−11	3.96e−11
7	0.0035	79500	0.459	21.6	0.1018	0.5391	5.59e−07	2.39e−10	1.12e−10	6.14e−11	1.97e−11
8	0.0035	79600	0.463	22.8	0.0994	0.5602	5.81e−07	2.44e−10	1.47e−10	9.44e−11	1.26e−11
9	0.0035	79400	0.467	23.1	0.0988	0.4904	5.09e−07	1.67e−10	1.01e−10	5.58e−11	1.99e−11
10	0.0035	80100	0.467	23.7	0.0976	0.6138	6.37e−07	2.23e−10	1.20e−10	6.51e−11	2.40e−11
Mean		79540	0.464	22.8	0.0994	0.5570	5.78e−07	2.32e−10	1.22e−10	6.81e−11	2.32e−11
Std		365	0.003	0.8	0.0015	0.0463	4.81e−08	4.27e−11	1.78e−11	1.51e−11	1.01e−11
CV		0.4	0.7	3.4	1.54	8.3	8.3	18.5	14.6	22.2	43.5
11	0.0040	78600	0.410	23.5	0.0980	1.2602	1.31e−06	4.31e−10	2.35e−10	9.79e−11	1.02e−10
12	0.0040	78600	0.406	24.2	0.0967	1.2434	1.28e−06	4.79e−10	2.85e−10	1.03e−10	1.64e−10
13	0.0040	78900	0.407	24.8	0.0958	1.6336	1.69e−06	5.92e−10	3.01e−10	1.60e−10	6.38e−11
14	0.0040	78600	0.408	24.2	0.0968	1.7146	1.78e−06	5.00e−10	2.93e−10	1.03e−10	1.81e−10
15	0.0040	78300	0.410	23.9	0.0973	1.3330	1.38e−06	5.26e−10	2.83e−10	1.73e−10	2.82e−11
Mean		78600	0.408	24.1	0.0969	1.4370	1.49e−06	5.06e−10	2.79e−10	1.27e−10	1.08e−10
Std		212	0.002	0.5	0.0008	0.2209	2.31e−07	5.96e−11	2.58e−11	3.61e−11	6.49e−11
CV		0.3	0.4	2.0	0.8	15.4	15.5	11.8	9.2	28.3	60.2

Table 4. Anisotropy ratio, principal permeability components in 1–2 coordinate system, and ratio of $a = K_s/K_{uns}$.

Exp.#	Ku1	Ku2	Beta (degrees)	Ku1/Ku2	Ks1	Ks2	A (= ratio of Ks/Ku)
1	8.19e−11	1.63e−11	10.5	5.041	3.55e−11	7.04e−12	0.433
2	7.52e−11	1.62e−11	8.3	4.635	4.35e−11	9.39e−12	0.579
3	8.47e−11	2.74e−11	8.1	3.090	5.99e−11	1.94e−11	0.707
4	8.73e−11	2.77e−11	9.8	3.145	7.05e−11	2.24e−11	0.808
5	1.20e−10	3.05e−11	0.1	3.934	1.81e−11	4.60e−12	0.151
Mean	8.98e−11	2.36e−11	7.4	3.969	4.55e−11	1.26e−11	0.536
Std	1.75e−11	6.84e−12	4.2	0.873	2.05e−11	7.87e−12	0.257
CV	1.94e+01	2.89e+01	56.8	21.985	4.51e+01	6.26e+01	47.957
6	3.14e−10	6.25e−11	9.2	5.026	2.25e−10	4.48e−11	0.718
7	2.47e−10	6.09e−11	6.1	4.061	1.86e−10	4.57e−11	0.751
8	2.47e−10	9.40e−11	4.7	2.625	1.55e−10	5.91e−11	0.628
9	1.77e−10	5.48e−11	9.5	3.236	1.53e−10	4.72e−11	0.862
10	2.35e−10	6.42e−11	8.1	3.662	1.96e−10	5.35e−11	0.834
Mean	2.44e−10	6.73e−11	7.5	3.722	1.83e−10	5.01e−11	0.759
Std	4.87e−11	1.54e−11	2.1	0.903	3.01e−11	6.09e−12	0.094
CV	2.00e+01	2.28e+01	27.5	24.3	1.65e+01	1.22e+01	12.4
11	5.44e−10	9.35e−11	13.5	5.824	5.19e−10	8.91e−11	0.953
12	7.14e−10	9.62e−11	16.0	7.423	7.12e−10	9.59e−11	0.997
13	6.25e−10	1.58e−10	7.9	3.965	4.69e−10	1.18e−10	0.750
14	7.74e−10	9.60e−11	16.2	8.064	1.12e−09	1.39e−10	1.450
15	5.33e−10	1.72e−10	4.5	3.092	3.43e−10	1.11e−10	0.645
Mean	6.38e−10	1.23e−10	11.6	5.674	6.33e−10	1.11e−10	0.959
Std	1.05e−10	3.85e−11	5.2	2.144	3.03e−10	1.96e−11	0.310
CV	1.65e+01	3.13e+01	44.8	37.783	4.79e+01	1.77e+01	32.344

direction is higher than in the y direction, primarily due to larger void channels between fiber bundles aligned parallel to the x axis compared to those aligned along the y axis. While the stitches used to bind the two uniaxial layers may partially obstruct flow channels in y-direction more than in x-direction, this effect is expected to be minor. The decreasing trend in anisotropy ($K_{uns,1}/K_{uns,2}$) with increasing V_f is assumed to result from non-proportional declines in the effective channel sizes (and thus porosities) along the channels in the principal 1- and 2-directions (and similarly x- and y-directions). This may be interpreted as the anisotropy ratio approaching a converged value as V_f approaches its limit.

- For the same fabric (Metyx LT850 0/90), our results qualitatively agree with a previous study whose anisotropy ratio (the ratios of $\frac{K_{uns,xx}}{K_{uns,yy}}$ within the same fiber volume fraction domain (41–55%)) ranged from 3.16 to 3.78.[23]

Steady-state characterization

Experimentally recorded rate of change in mass, dm/dt was utilized to determine 2D steady permeability of the fabric as discussed earlier. Figure 11 illustrates the pressure and velocity fields for one sample case, Experiment 7. It highlights how the pressure distribution develops across the domain and how a significant velocity gradient forms, particularly near the inlet. The graphical presentation qualitatively demonstrates that the numerical model successfully captures physically meaningful behavior for steady flow through an anisotropic porous medium.

- Principal permeability components: As shown in Table 4 and Figure 12, $K_{s,1}$ was measured as $6.3 \pm 3.0 \times 10^{-10}$, $1.9 \pm 0.3 \times 10^{-10}$ and $4.6 \pm 2.1 \times 10^{-11}$ m^2 and $K_{s,2}$ was measured as $1.1 \pm 0.2 \times 10^{-10}$, $5.0 \pm 0.6 \times 10^{-11}$ and $1.2 \pm 0.8 \times 10^{-11}$ m^2 at $V_f = 0.408 \pm 0.002$, $V_f = 0.464 \pm 0.003$ and $V_f = 0.543 \pm 0.007$, respectively.

Comparison of the steady-state and unsteady-state permeabilities

As listed in Table 4, the **ratio of steady to unsteady permeabilities**, $\frac{K_{s,xx}}{K_{uns,xx}} = \frac{K_{s,yy}}{K_{uns,yy}} = \frac{K_{s,xy}}{K_{uns,xy}} = \frac{K_{s,1}}{K_{uns,1}} = \frac{K_{s,2}}{K_{uns,2}} = \text{constant} \equiv a$ was determined as 0.97 ± 0.33, 0.76 ± 0.09 and 0.54 ± 0.26 at $V_f = 0.408 \pm 0.002$, $V_f = 0.464 \pm 0.003$ and $V_f = 0.543 \pm 0.007$, respectively.

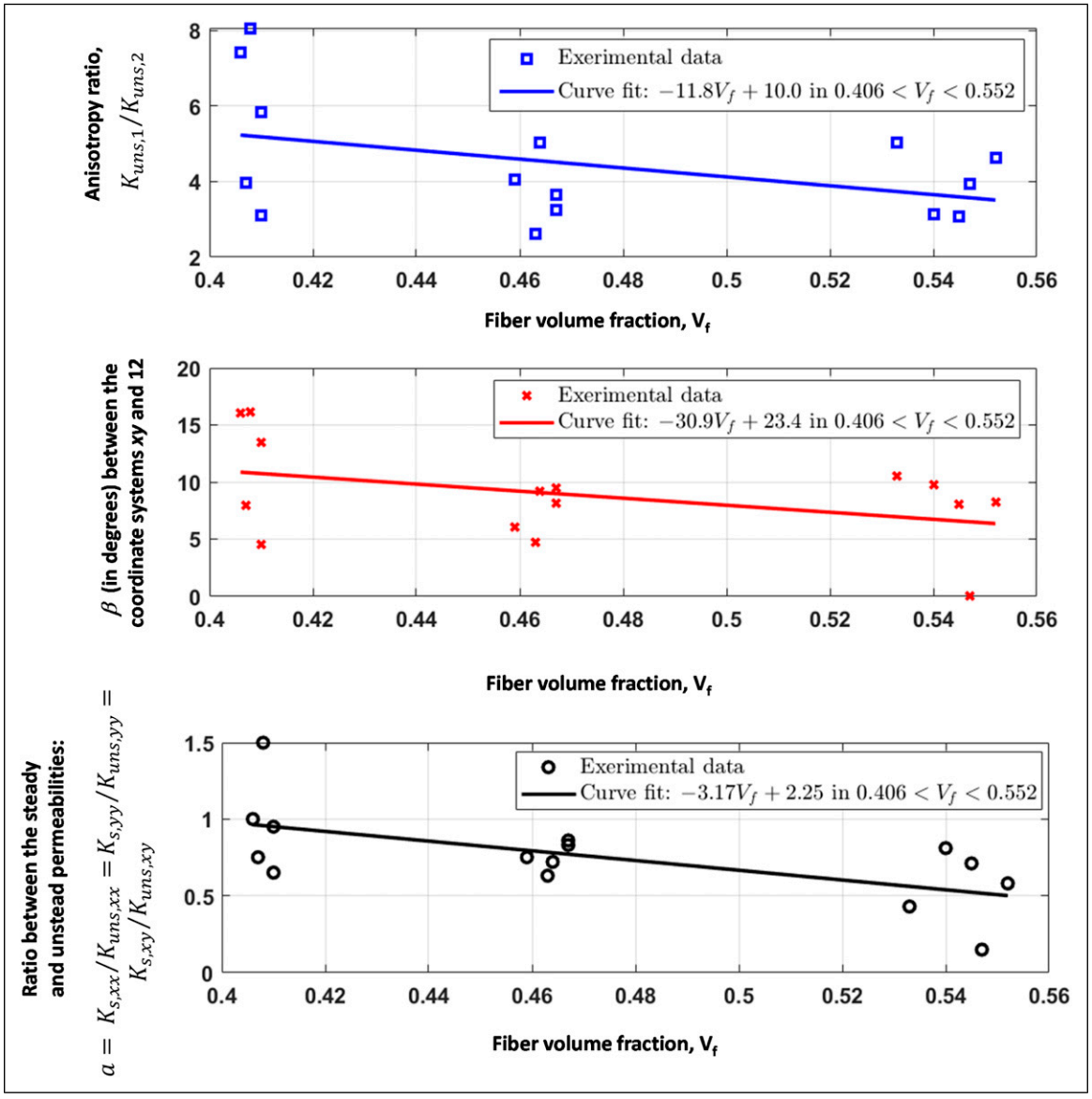


Figure 10. Analysis of the results; (top): anisotropy ratio, $K_{uns,1}/K_{uns,2}$; (mid) the rotation angle, β between *x*–*y* and 1–2 coordinate planes; and (bottom) the ratio between the steady and unsteady permeabilities: $a = \frac{K_{s,xx}}{K_{uns,xx}} = \frac{K_{s,yy}}{K_{uns,yy}} = \frac{K_{s,xy}}{K_{uns,xy}}$

- Although most findings in the literature report $K_s > K_{uns}$, some studies have documented the opposite trend ($K_s < K_{uns}$). Our results are consistent with this latter group. The contrasting outcomes reported in the literature can be attributed to differences in fiber architecture (type of fabric), fiber volume fraction range, void formation, flow rheology, and measurement methods. Capillary suction during unsaturated flow and microvoid formation within intra-tow regions may contribute to these discrepancies. In this study, the ratio K_s/K_{uns} decreased with increasing V_f, which may be linked not only to some of the above-mentioned effects, but also to nesting and fiber rearrangement during increasing compaction, which may reduce flow channels non-proportionally: more significantly in the steady state than in the unsteady regime.
- This study does not provide definitive evidence for some behaviors (such as why anisotropy and the ratio of K_s/K_{uns} decrease with V_f), however more experiments and validating simulations on small scale unit cells of fiber structures will help understanding these issues in the future studies.
- The **curve fit** to the discrete experimental data in Figure 12 was determined by relating permeability, K to fiber volume fraction, V_f in the following exponential form: $K = Ae^{-BV_f}$. The

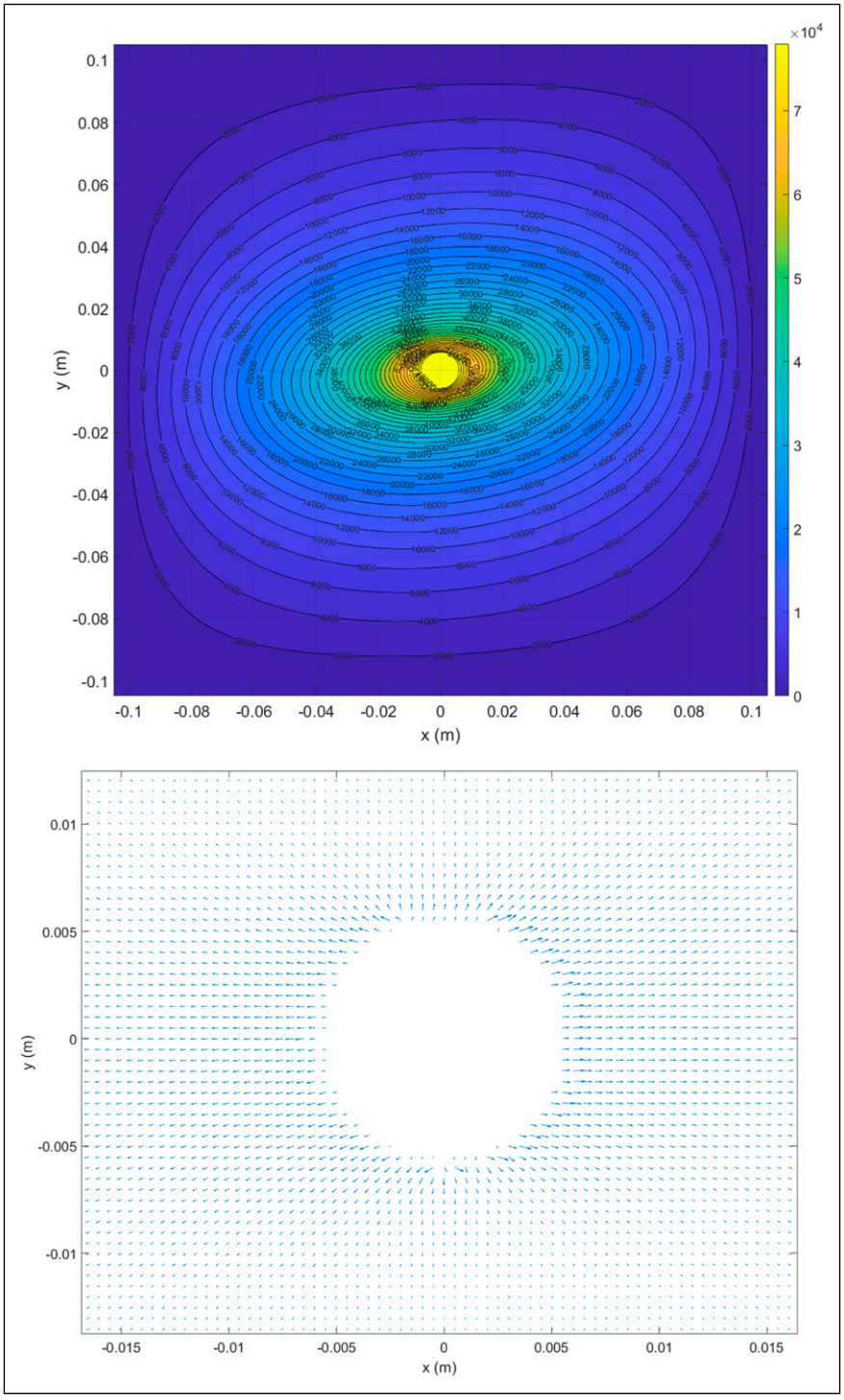


Figure 11. Numerically determined steady-state pressure distribution, $P(x,y)$ in Pascals (top) and velocity field (bottom; around the inlet hole was shown here) for Experiment 7.

constants A and B were obtained using a least-square method, and shown in the legend of the figure with the following units: $[A] = m^2$ and $[B] = 1$.

- Table 4 and Figure 12 show principal permeability components during both unsteady and steady flow regimes. They showcase two important observations: (i) a **strong anisotropy ratio**, $K_{uns,1}/K_{uns,2}$

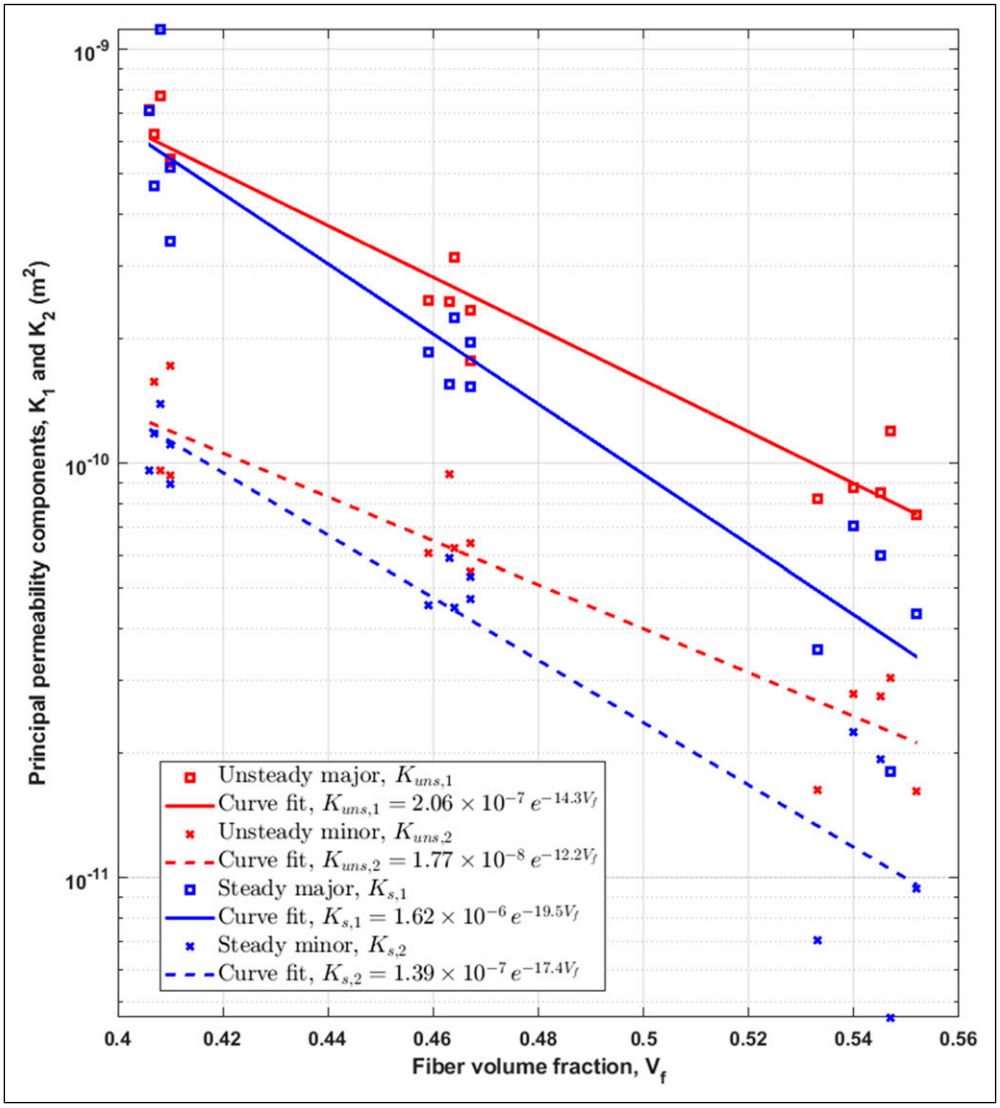


Figure 12. Principal components of unsteady and steady permeabilities of the fabric preform.

(approximately, $K_{uns,1} \cong 4-6\,K_{uns,2}$), and (ii) **steady permeability is smaller than the unsteady permeability** ($K_s \cong 0.4-1.0\,K_{uns}$ in 13 experiments out of 15; however two outlier experiments yielded $\frac{K_s}{K_{uns}} = 0.151$ and 1.45 for Experiments 5 and 14, respectively).

- Although there is considerable scatter in the experimental data (which is commonly observed in the literature and typically attributed to the non-uniformity of the fabric structure and the variability in fiber bundle placement during cutting and manual assembly), the general trend in β (rotation of the 12 system relative to the xy system) shows a decrease with increasing fiber volume fraction, which is consistent with the trends observed for the anisotropy ratio ($K_{uns,1}/K_{uns,2}$) and a.

Comparison with literature

In general, $\frac{K_s}{K_{uns}}$ result presented here is in good agreement with many previous studies.

- Yenilmez et al.[24] and Yalcinkaya et al.[25] utilized the same biaxial fabric as this study. When used in Vacuum Assisted Resin Transfer Molding (VARTM), both previous studies found that the arrival of the flow front led to a reduction in thickness, caused by increased fiber nesting due to the lubrication effect. Consequently, the unsteady permeability of this biaxial fabric was anticipated to be higher than the steady permeability.
- Yalcinkaya et al.[15] reported that the unsteady 1D permeability of same biaxial fabric (eight layers of

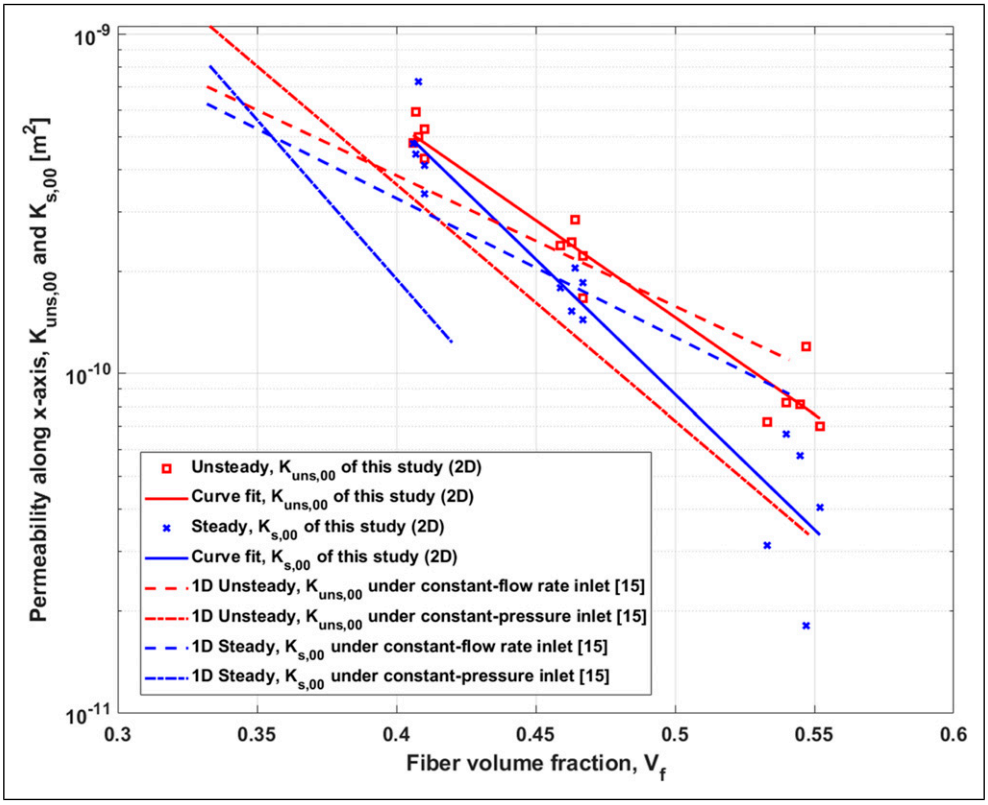


Figure 13. Comparison of the results from this study for 5-layer specimens under 2D (radial) experiments with those from a previous study by Yalcinkaya et al.[15] for 8-layer specimens under 1D experiments, using the same fabric. Note that only the permeability component along the *x*-axis was compared, as their analysis was conducted exclusively in that direction.

biaxial fabric in a domain of V_f = 41–55%) was greater than the steady permeability, with a $\frac{K_{uns}}{K_s}$ ratio ranging from 2.01 to 4.38 (or, in terms of the inverse ratio used here in this study, $0.23 < \frac{K_s}{K_{uns}} < 0.50$). The comparison of permeability results along the *x*-axis between the 5-layer specimens in this study and the 8-layer specimens from Yalcinkaya et al.[15] is shown in Figure 13. Note that Yalcinkaya et al.'s analysis was conducted under two different boundary conditions: (1) constant-pressure inlet and (2) constant-flow-rate inlet. While their two conditions produced some similar trends, notable variations were also observed. This difference, along with the scatter observed in our five repeated experiments for statistical analysis, highlights a commonly reported variation in permeability measurements in the literature—not only among different researchers, but also across repeated experiments by the same researcher. It is worth emphasizing that previous studies by Yenilmez et al.[24] and Yalcinkaya et al.[15,25] used 1D characterization. However, the experimental procedure was time-consuming (approximately twice) than 2D radial permeability analysis employed in this study. For example, assuming skilled personnel and appropriate instruments, performing two separate 1D experiments along x- and y-directions typically requires around 2 h. In contrast, a single 2D radial test can be completed in approximately 1 h and simultaneously provides the in-plane permeability components, making the radial test more time-efficient overall.

- Diallo et al.[26] found the steady permeability consistently smaller than the unsteady permeability. On the other hand, another study[27] indicated that the ratio of average unsteady permeability to steady permeability $\frac{K_{uns}}{K_s}$ fell within the range of 0.4 to 1.6 (i.e., $0.63 < \frac{K_s}{K_{uns}} < 2.5$) depending on the fabric type (bidirectional, random and unidirectional fabrics).

Conclusions

The 2D permeability of a 5-layer biaxial fabric preform was investigated under radial flow and central constant-injection pressure boundary condition at fiber volume fractions of V_f = 41–54%. The unsteady permeability, K_{uns} was measured by using a conventional approach previously presented in literature by tracking flow front along three directions (production direction of the fabric roll (*x*),

transverse direction (y) and $\theta = 45°$). The results demonstrated that the permeability of the biaxial fabric is anisotropic, with higher permeability in the x-direction significantly higher than in the y-direction. This anisotropy and thus preferential pathways for resin flow could be attributed to larger space between the fiber bundles placed parallel to the production axis than the ones parallel to the transverse direction.

For steady permeability, a straightforward but yet effective approach was proposed here in this study. It was a combination of experimental data (flow rate) and an iterative numerical analysis. Steady permeability of a porous fiber structure is needed for stages such as resin-bleeding that takes place after resin arrival to all exit vents and thus steady resin flow occurs. This study will be helpful to measure 2D steady permeability components with the following steps: (1) it is assumed that the anisotropy ratio of unsteady permeability components and the rotation angle between x–y and principal 1–2 axes remains unchanged at steady state, and (2) permeability values are numerically iterated by calculating exit velocity components along all edges and matching the corresponding outflow rate ($Q_{\text{numerical}}$) to the experimentally measured flow rate in the characterization experiment ($Q_{\text{experiment}}$). Our characterization approach provides a time-saving approach for analyzing anisotropic preforms (compared to a set of 1D characterization experiments which are approximately twice time-consuming to conduct).

The anisotropy ratio, $K_{uns,1}/K_{uns,2}$ was determined as 5.67 ± 2.14, 3.72 ± 0.90, and 3.97 ± 0.87 at $V_f = 0.41$, 0.46 and 0.54, respectively.

All experiments except one (14 out of 15 experiments) resulted in a smaller steady permeability than the unsteady permeability. The ratio of steady to unsteady permeabilities, $\frac{K_s}{K_{uns}}$ was determined as 0.97 ± 0.33, 0.76 ± 0.09, and 0.54 ± 0.26 at $V_f = 0.41$, 0.46 and 0.54, respectively.

To assess the scatter of permeability values, we calculated the variation with standard deviation (std) and coefficient of variation (CV) as presented in Tables 3 and 4. Various potential sources contributing to this observed scatter can be due to (1) fabric deformation during sample preparation, (2) material non-uniformity (caused by the irregular fabric roll and varying nesting of fabric layers during the stacking and compaction), and (3) non-repeatable labor (cutting and placement).[19,28,29]

In summary, this study provides valuable insights into the permeability behavior of biaxial fabric preforms. The proposed numerical solution allows determining in-plane steady state permeability calculation for circular or square molds (even though the flow front propagation and pressure distribution are elliptical). It provides straightforward computation of numerical volumetric outflow rate by using the unsteady permeability tensor, and then scales it to match the experimental flow rate. This approach can be utilized to improve the design and manufacturing of composite structures, especially during the resin bleeding (which is a quasi-steady control action usually used to settle the pressure and thickness distribution). The novel numerical approach presented here offers a promising tool for straightforward and yet effective permeability characterization of anisotropic materials, enhancing the understanding and prediction of composite manufacturing processes.

ORCID iDs

Hasan Caglar https://orcid.org/0000-0001-5565-9839
Ercument Murat Sozer https://orcid.org/0000-0001-7327-5628

Funding

The authors received no financial support for the research, authorship, and/or publication of this article.

Declaration of conflicting interests

The authors declared no potential conflicts of interest with respect to the research, authorship, and/or publication of this article.

Data Availability Statement

Data sharing not applicable to this article as no datasets were generated or analyzed during the current study.

References

1. Miranda Campos B, Bourbigot S, Fontaine G, et al. Thermoplastic matrix-based composites produced by resin transfer molding: a review. *Polym Compos* 2022; 43(5): 2485–2506.
2. Obande W, Mamalis D, Ray D, et al. Mechanical and thermomechanical characterisation of vacuum-infused thermoplastic-and thermoset-based composites. *Mater Des* 2019; 175: 107828.
3. Obande W, Ó Brádaigh CM and Ray D. Thermoplastic hybrid-matrix composite prepared by a room-temperature vacuum infusion and in-situ polymerisation process. *Compos Commun* 2020; 22: 100439.
4. Advani SG and Sozer EM. *Process modeling in composites manufacturing*. CRC Press, 2002.
5. Sas HS, Šimáček P and Advani SG. A methodology to reduce variability during vacuum infusion with optimized design of distribution media. *Compos Appl Sci Manuf* 2015; 78: 223–233.
6. Konstantopoulos S, Hueber C, Antoniadis I, et al. Liquid composite molding reproducibility in real-world production of fiber reinforced polymeric composites: a review of challenges and solutions. *Adv Manuf Polym Compos Sci* 2019; 5(3): 85–99.
7. Syerko E, Schmidt T, May D, et al. Benchmark exercise on image-based permeability determination of engineering

textiles: microscale predictions. *Compos Appl Sci Manuf* 2023; 167: 107397.
8. Becker D and Mitschang P. Influence of preforming technology on the out-of-plane impregnation behavior of textiles. *Compos Appl Sci Manuf* 2015; 77: 248–256.
9. Endruweit A, Luthy T and Ermanni P. Investigation of the influence of textile compression on the out-of-plane permeability of a bidirectional glass fiber fabric. *Polym Compos* 2002; 23(4): 538–554.
10. Pierce RS. Challenges in permeability characterisation for modelling the manufacture of wind turbine blades. *IOP Conf Ser Mater Sci Eng* 2023; 1293(1): 012009.
11. Maguire J, Doyle A and Brádaigh CÓ. Process modelling of thick-section tidal turbine blades using low-cost fibre reinforced polymers. In: Proceedings of the 12th European wave and tidal energy conference, Cork, Ireland, 27 August–2 September 2017.
12. Maguire JM, Nayak K and Ó Brádaigh CM. Characterisation of epoxy powders for processing thick-section composite structures. *Mater Des* 2018; 139: 112–121.
13. Maguire JM, Simacek P, Advani SG, et al. Novel epoxy powder for manufacturing thick-section composite parts under vacuum-bag-only conditions. Part I: through-thickness process modelling. *Compos Appl Sci Manuf* 2020; 136: 105969.
14. Gardiner G. Resin-infused MS-21 wings and wingbox. *Composites World* 2014. [Online]. Available: https://www.compositesworld.com/articles/resin-infused-ms-21-wings-and-wingbox (accessed 03 February 2024).
15. Yalcinkaya MA, Sarioglu A and Sozer EM. A novel mold design for one-continuous permeability measurement of fiber preforms. *J Reinf Plast Compos* 2015; 34(11): 915–930.
16. Swery EE, Allen T, Comas-Cardona S, et al. Efficient experimental characterisation of the permeability of fibrous textiles. *J Compos Mater* 2016; 50(28): 4023–4038.
17. Buntain MJ and Bickerton S. Compression flow permeability measurement: a continuous technique. *Composites Part A: Appl Sci Manuf* 2003; 34(5): 445–457.
18. Comas-Cardona S, Binetruy C and Krawczak P. Unidirectional compression of fibre reinforcements. Part 2: a continuous permeability tensor measurement. *Compos Sci Technol* 2007; 67(3–4): 638–645.
19. May D, Aktas A, Advani S, et al. In-plane permeability characterization of engineering textiles based on radial flow experiments: a benchmark exercise. *Composites Part A: Appl Sci Manuf* 2019; 121: 100–114.
20. Fauster E, Berg DC, May D, et al. Robust evaluation of flow front data for In-Plane permeability characterization by radial flow experiments. *Adv Manuf Polym Compos Sci* 2018; 4(1): 24–40.
21. Weitzenböck JR, Shenoi RA and Wilson PA. Radial flow permeability measurement. Part A: theory. *Composites Part A: Appl Sci Manuf* 1999; 30(6): 781–796.
22. Chan AW and Hwang S-T. Anisotropic in-plane permeability of fabric media. *Polym Eng Sci* 1991; 31(16): 1233–1239.
23. Caglar B, Hancioglu M and Sozer EM. Monitoring and modeling of part thickness evolution in vacuum infusion process. *J Compos Mater* 2021; 55(8): 1053–1072.
24. Yenilmez B and Sozer EM. Compaction of e-glass fabric preforms in the vacuum infusion process:(a) use of characterization database in a model and (b) experiments. *J Compos Mater* 2013; 47(16): 1959–1975.
25. Yalcinkaya MA, Caglar B and Sozer EM. Effect of permeability characterization at different boundary and flow conditions on vacuum infusion process modeling. *J Reinf Plast Compos* 2017; 36(7): 491–504.
26. Diallo ML, Gauvin R and Trochu F. Key factors affecting the permeability measurement in continuous fiber reinforcements. In: Proceedings of ICCM, 1997, Vol. 11. Gold Coast, Queensland, Australia, July 14th-18th, 1997.
27. Bréard J, Henzel Y, Trochu F, et al. Analysis of dynamic flows through porous media. Part I: comparison between saturated and unsaturated flows in fibrous reinforcements. *Polym Compos* 2003; 24(3): 391–408.
28. Hoes K, Dinescu D, Sol H, et al. Study of nesting induced scatter of permeability values in layered reinforcement fabrics. *Composites Part A: Appl Sci Manuf* 2004; 35(12): 1407–1418.
29. Sarioglu A. *Permeability measurement experiments for fabric preforms used in LCM processes*. MSc Thesis, Koç University, 2012.

Appendix

Nomenclature

a	steady/unsteady permeabilities ratio
h	mold cavity thickness (= thickness of a specimen)
$[K]$	permeability tensor
$K_{s,1}$, $K_{uns,1}$	higher steady and unsteady in-plane principal permeability component
$K_{s,2}$, $K_{uns,2}$	lower steady and unsteady in-plane principal permeability component (perpendicular to K_1)
K_{fit}	permeability computed with curve-fitting
$K_{s,xx}$, $K_{s,yy}$	steady permeability components along x- and y-directions, respectively

$K_{uns,xx}$, $K_{uns,xy}$, $K_{uns,45}$, $K_{uns,yy}$	unsteady permeability components along x-, xy-, 45° and y-directions, respectively
$\dot{m}$	mass flow rate
n	number of fabric layers used in a stacked specimen
P	resin pressure
P_{inj}	injection pressure at the inlet hole
Q_{exp}	experimental volumetric flow rate
Q_{num}	numerical volumetric flow rate
$r_{f,xx}$, $r_{f,45°}$, $r_{f,yy}$	flow front radii along x, $\theta = 45°$ and y directions
r_i	inlet hole radius
T	average temperature of resin during the experiment
t	time
$\overline{U}$	Darcy's resin velocity
V_f	fiber volume fraction
∇P	resin pressure gradient
β	angle of rotation of principal axis 1 relative to the production direction of the fabric (x-direction)
μ	resin viscosity
ϕ	porosity
ρ_{bulk}	bulk density of glass fibers
ρ_{sup}	superficial density of fabric per layer